Received: 22 October 2023 | Revised: 12 December 2023 | Accepted: 13 December 2023

DOI: 10.1002/app.55137

RESEARCH ARTICLE

Applied Polymer SCIENCE WILEY

Flame retardant biogenic building insulation materials from hemp fiber

Porus Sunil Jadhav | **Arpita Sarkar** | **Long Zhu** | **Shenqiang Ren**

Department of Materials Science and Engineering, University of Maryland (UMD), College Park, Maryland, USA

Correspondence
Shenqiang Ren, Department of Materials Science and Engineering, University of Maryland (UMD), College Park, MD 20742, USA.
Email: sren@umd.edu

Funding information
Advanced Research Projects Agency - Energy, Grant/Award Number: DE-AR0001771

Abstract

Biogenic thermal insulation materials are in high demand because of its carbon-sequestration nature. However, high flammability, moisture condensation, and relatively high thermal conductivity of biogenic material are major concerns for sustainable building applications. In this study, we report the fire-retardant cellulose xerogel insulation nanocomposites derived from hemp fiber recycling and silica xerogel, in which the boric acid treatment improves its fire retardancy. The as-prepared materials show a low thermal conductivity of 31.3 mW/m K, high flexural modulus of 665 MPa, hydrophobicity with the water contact angle of 115°, and fire retardancy with 30% weight loss over a period of burning time 10 min. Overall, this work provides an effective method for the synthesis of fire-retardant biogenic thermal insulation materials and shows a promising way for next-generation bio-based insulation materials.

KEYWORDS

biogenic, fire retardancy, hemp fiber, thermal insulation materials, xerogel composites

1 | INTRODUCTION

The development of next-generation insulation materials based on biogenic products has gained immense interest due to the current environmental strive for eco-efficiency, sustainability, and industrial ecology.[1] Biogenic materials are renewable, sustainable in carbon footprint, and utilized to limit environmental impact.[2,3] Moreover, they possess a smaller ecological impact when compared with conventional materials, thereby decreasing waste production and lessening reliance on new resources.[4] Among the biogenic materials, hemp fiber is known for its carbon-sequestering ability, abundant production, excellent mechanical strength, and biodegradability.[5–7] However, the major drawbacks of agriculture waste products like hemp are its relatively high thermal conductivity, moisture condensation, and flammability, which hinder their use in potential green building applications.[8–11] Therefore, a significant improvement in flame retardancy and thermal resistance is required without compromising its mechanical properties and carbon sequestration nature to meet the safety and sustainability requirements. Here, we report recycling of hemp fiber and its cellulose-reinforced silica xerogel composites for building insulation applications. Sodium hydroxide pretreatment along with boric acid onto hemp fibers is used to remove lignin and hemicellulose and improve the fire retardancy of the recycled hemp-derived cellulose nanocomposites. In this regard, boric acid delivers char-forming benefits while the decomposition of the melted boric acid helps to reduce air oxidation.[12,13] Furthermore, the boric acid also facilitates hydrolysis to remove lignin and hemicellulose from hemp fiber. The as-prepared nanocomposites display a low thermal conductivity of 31.3 mW/m K, a

flexural modulus of 665 MPa, hydrophobicity with water contact angle of 115°, and recyclability of 92% along with excellent fire retardancy. Overall, the as-prepared fire-retardant cellulose-xerogel nanocomposite coming from biogenic agriculture waste could lay the establishment of next-generation bio-based insulation materials.

2 | RESULTS AND DISCUSSION

Hemp fibers are composed of 52%–91% cellulose, 4%–18% hemicellulose, 1%–21% lignin, and 1%–17% pectin.[14] The cellulose is arranged into microfibrils that are cross-linked by glycans and are made up of linear chains of β-1,4-linked D-glucose units.[15] The cross-linked networks of glycans and microfibrils are further surrounded in a matrix of pectic substances and reinforced with structural aromatic substances such as hydroxycinnamates and lignin.[16] Therefore, chemical pre-treatment is necessary to remove the noncellulosic part from the hemp fibers. Figure 1 shows the schematic diagram of the alkaline pretreatment (NaOH) followed by acid hydrolysis (HCl and boric acid) of the hemp fibers. Alkaline pretreatment effectively disrupts the cell wall and removes lignin and pectin substances thus producing cellulose-rich residue while the acid hydrolysis further removes hemicellulose. Figure 1b,c shows the images of raw hemp fibers and NaOH-HCl-treated hemp fibers, respectively. The scanning electron microscopy (SEM) images of hemp fibers, NaOH treated, NaOH-HCl treated, and NaOH-boric acid-treated hemp fibers are shown in Figure 1d,e and S1. Figures 1e and S1b reveal the smoother surface of hemp fiber after NaOH-HCl and NaOH-boric acid treatment, which signifies the effective removal of lignin, pectin, and hemicellulose. Figure 1f depicts the Fourier-transform infrared spectroscopy (FTIR) spectra of NaOH-treated, NaOH-HCl treated, and NaOH-boric acid-treated hemp fibers. The FTIR spectra show a broad peak at approximately 3298 cm^{-1} in all cases, indicating the presence of hydroxyl groups (—OH) in the treated hemp fibers. The peak intensity at 3298 cm^{-1} is significantly higher in the case of NaOH-HCl-treated and NaOH-boric acid-treated fibers as compared with NaOH-treated fibers, indicating an increased proportion of cellulose

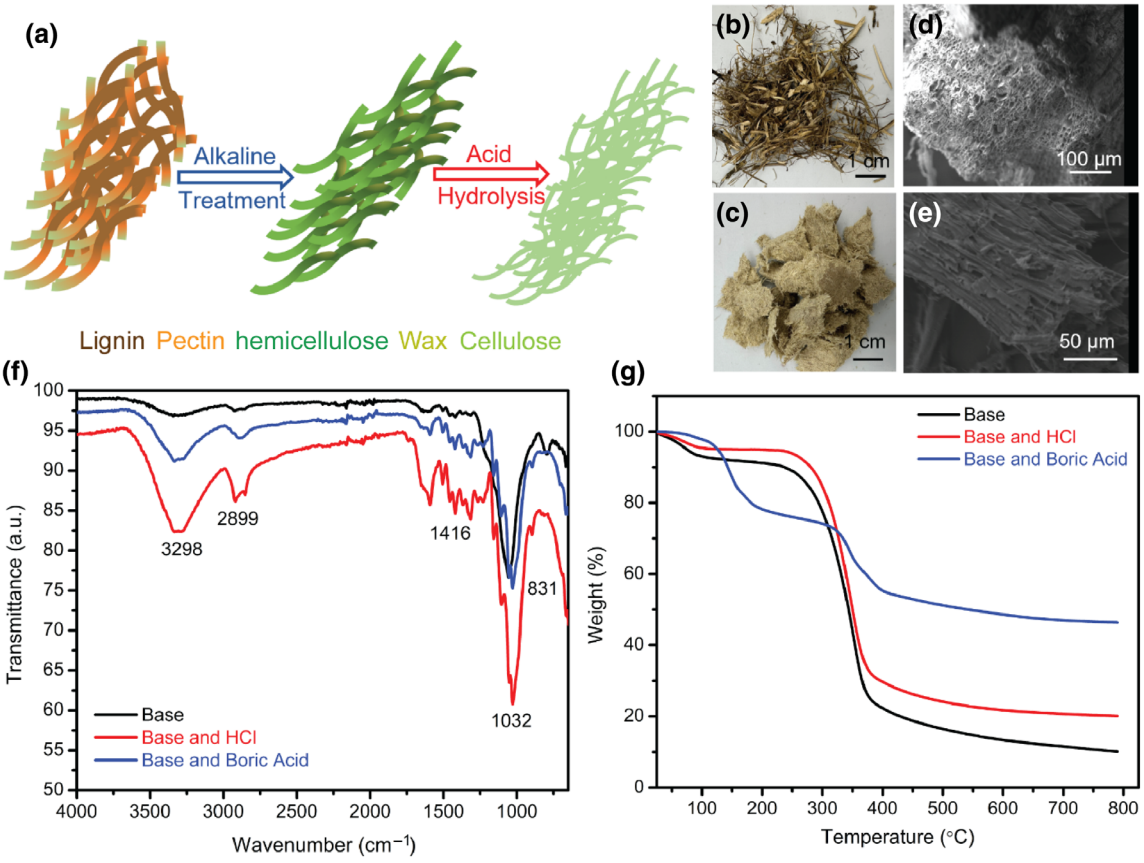

FIGURE 1 (a) Schematic diagram of hemp fiber treatments, (b) image of raw hemp fiber, (c) image of NaOH-HCl treated hemp fibers, (d) scanning electron microscopy (SEM) image of raw hemp fiber, (e) SEM image of NaOH-HCl treated hemp fibers, (f) Fourier-transform infrared spectroscopy spectra of different treatments of hemp fibers, and (g) thermogravimetric analysis curves of different treatment of hemp fibers. [Color figure can be viewed at wileyonlinelibrary.com]

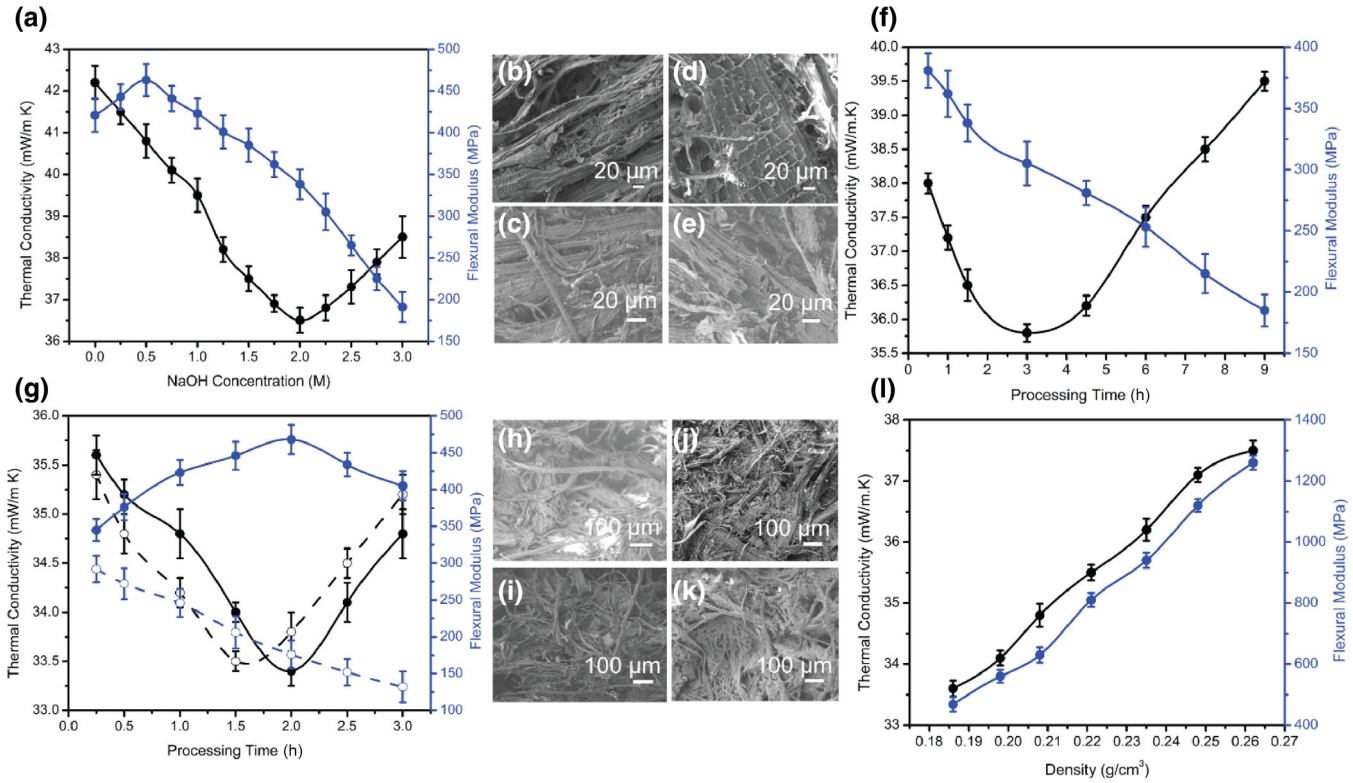

FIGURE 2 (a) Thermal conductivity versus flexural modulus plot of hemp fibers with different concentrations of NaOH treatment, (b) scanning electron microscopy (SEM) image of 1 M NaOH treated hemp fiber. (c) SEM image of 2 M NaOH treated hemp fiber, (d) SEM image of 1 h NaOH (2 M) treated hemp fiber, (e) SEM image of 3 h NaOH (2 M) treated hemp fiber, (f) thermal conductivity versus flexural modulus plot of 2 M NaOH treated hemp fibers for different processing times, (g) thermal conductivity and flexural modulus plot of NaOH-boric acid and NaOH-HCl treated hemp fibers varying different processing times, (h) SEM image of 30 min NaOH-HCl treated hemp fibers, (i) SEM image of 1 h NaOH-HCl treated hemp fibers, (j) SEM image of 30 min NaOH-boric acid treated hemp fiber, (k) SEM image of 2 h NaOH-boric acid treated hemp fibers, and (l) density-dependent study of NaOH-boric acid treated hemp fibers. [Color figure can be viewed at wileyonlinelibrary.com]

after NaOH-HCl and NaOH-boric acid treatment. Additionally, a peak at around 2899 cm^{-1} indicates the existence of methyl (—CH_3) and methylene (—CH_2) groups in the hemp fiber. Furthermore, the small band related to the C—O stretching and C—H bending in hemicellulose shifted to a higher wavenumber for the treated hemp fibers, suggesting the removal of hemicellulose from the surface after alkaline treatment followed by the acid hydrolysis. The thermal stability of the NaOH-treated, NaOH-HCl treated, and NaOH-boric acid-treated hemp fibers are investigated by thermogravimetric analysis (TGA) and shown in Figure 1g. In the case of NaOH-treated and NaOH-HCl-treated fiber, the TGA curve shows two distinct weight loss steps. The initial weight loss at below 100°C is due to the moisture evaporation of the cellulose materials. The second major weight loss between 200 and 400°C corresponds to the degradation of cellulose. On the other hand, NaOH-boric acid-treated hemp fibers clearly show three distinct thermal decomposition steps. The first decomposition step between 50 and 190°C is due to the moisture absorption of borax. The second decomposition step between 250 and 360°C occurred due to the cellulose degradation and the third decomposition step between 360 and 440°C indicates the complex formation between boron and cellulose. The final residue for the NaOH-boric acid-treated sample is around 46% which is significantly higher than that of NaOH-HCl (20%) treated and NaOH-treated hemp fibers (10%), indicating char formation at higher temperature (800°C) in the case of boric acid treated hemp fibers. Both generation of water from borax residue and char formation on cellulose surfaces play a key role to delay flame propagation and ignition.

Figure 2a shows the thermal conductivity change of NaOH-treated hemp fibers varying in different NaOH concentrations. The thermal conductivity decreases from 42.2 to 36.6 mW/m K with increasing NaOH concentration from 0.5 to 2 M, which indicates the removal of lignin, pectin, and hemicellulose from hemp fiber with increasing NaOH concentration. Figure 2b,c shows the

rigid and broken fibers in the case of 1 and 2 M NaOH treatment, respectively. However, further increase in NaOH concentration from 2 to 3 M results in decrease in thermal conductivity, which is due to the degradation and swelling of the cell wall and the formation of small pores on the surface of the fiber. The SEM images also reveal (Figure S2) the disruption and swelling of the cell wall and small pore diameter in the case of 2.5 and 3 M NaOH-treated hemp fibers. The optimum thermal conductivity of 36.6 mW/m K is observed in the case of 2 M NaOH treatment, which signifies the effective removal of the non-cellulosic part from hemp fibers. Figure 2a also displays the change in the flexural modulus of alkaline-treated hemp fibers with the variations in NaOH concentrations. A slight increase in flexural modulus is observed from 421 to 463 MPa with increasing NaOH concentration from 0 to 0.5 M and then shows a decreasing trend from 463 to 191 MPa with further increasing the NaOH concentration from 0.5 to 3 M. The initial increase in the flexural modulus can be attributed to the formation of fiber-to-fiber interface, improved surface interaction due to initial roughness, and an increase in cellulose content. However, after 0.5 M processing condition, the flexural modulus decreases because of the cell wall degradation, which also results in a decrease in its density (Figure S3). The 2 M NaOH treatment shows to be effective to remove lignin, pectin, and hemicellulose from hemp fibers, and therefore, we further studied the effect of time variation using 2 M NaOH treatment. Figure 2d,e shows the SEM images of 1-h NaOH-treated and 3-h NaOH-treated hemp fibers, respectively. Figure 2f represents the change in thermal conductivity and flexural modulus with varying different processing times from 0.5 to 9 h using 2 M NaOH concentration. Similar to the concentration-dependent study, there is a visible drop in thermal conductivity from 38 to 35.7 mW/m K with increasing the processing times from 0.5 to 3 h, and after that, it increases from 35.7 to 39.5 mW/m K. The initial decrease in thermal conductivity is due to the lignin and wax removal from the hemp fiber, which results in a decrease in density (Figure S4). However, after 3 h, the fibers get disintegrated and swell which result in an increase in thermal conductivity (Figures 2d,e and S5). The flexural modulus shows a decreasing trend from 381 to 185 MPa with increasing processing time from 0.5 to 9 h due to the decrease in density.

Figure 2g represents the comparison between NaOH treatment followed by HCl and boric acid for different processing time variations on hemp fibers. At first, the thermal conductivity decreases from 35.5 to 33.6 mW/m K for HCl treated samples as the treatment time increases from 0.25 to 1.5 h, then the thermal conductivity increases from 33.6 to 35.3 mW/m K as treatment time is increased from 1.5 to 3 h. Similarly, in the case of boric-acid treatment, thermal conductivity decreases from 35.7 to 33.4 mW/m K as treatment time is increased from 0.25 to 2 h and then increases from 33.4 to 34.7 mW/m K as the treatment time is increased from 2 to 3 h. In both cases, a noticeable decrease in thermal conductivity is observed because of the removal of hemicellulose, lignin, and pectin, which causes the reduction in the size of the hemp fibers (Figure 2h–k). There is a small difference observed in the case of the thermal conductivity change between HCl and boric acid treatment. The flexural modulus of boric acid-treated samples is higher than that of the HCl-treated fibers at different processing times. The increased flexural modulus is resulted from the morphology change and higher density of the boric acid-treated fibers. The SEM images of HCl-treated fibers also show smaller and more disintegrated fibers as compared with boric acid treatment (Figures S7 and S8). Figure 2f displays the density-dependent study for 2 M NaOH treatment for 3 h in the first step and boric acid treatment for 2 h in the second step of hemp fibers. Increasing density shows an increase in the mechanical strength of the treated fibers. The flexural modulus is increased from 464 to 1262 MPa with increasing density from 0.18 to 0.26 g/cm^3. Simultaneously, the increased density results in increasing the thermal conductivity of the treated hemp fibers from 33.6 to 37.5 mW/m K.

Furthermore, the hemp-derived cellulose-reinforced silica xerogel nanocomposites are prepared using NaOH-boric acid-treated hemp fibers with different wt% of water glass-based silica xerogel. Figure 3a displays the FTIR spectra of the different xerogel wt% of xerogel-cellulose nanocomposites. The FTIR spectra exhibit several characteristic peaks of cellulose, such as O—H stretching at 3335 cm^{-1}, C—H stretching at 2925 cm^{-1}, C—C and C—O stretching at 1625 and 1412 cm^{-1}, and C—O—C skeletal vibrations at 1054 cm^{-1}, respectively. The intensity of O—H stretching at 3335 cm^{-1} decreases with increasing xerogel concentration in the nanocomposites. Furthermore, a peak appeared at 780 cm^{-1} due to Si—O vibrations and an adjacent peak of 920 cm^{-1} coming from the rocking bending vibrations of Si—OH groups indicates the incorporation of silica xerogel in the nanocomposites. Figure 3b shows the thermal conductivity and flexural modulus of different xerogel concentrations of nanocomposites. The thermal conductivity of the composites decreases from 33.5 to 31.2 mW/m K with increasing the xerogel concentration from 5 to 40 wt% due to the increase in porosity and decrease in density (Figure S9). It is interesting to note that increasing xerogel wt% above 40 wt% results an increase of thermal conductivity due to the aggregation of silica xerogel particles (Figure 3c–e) which leads to a decrease in porosity. The

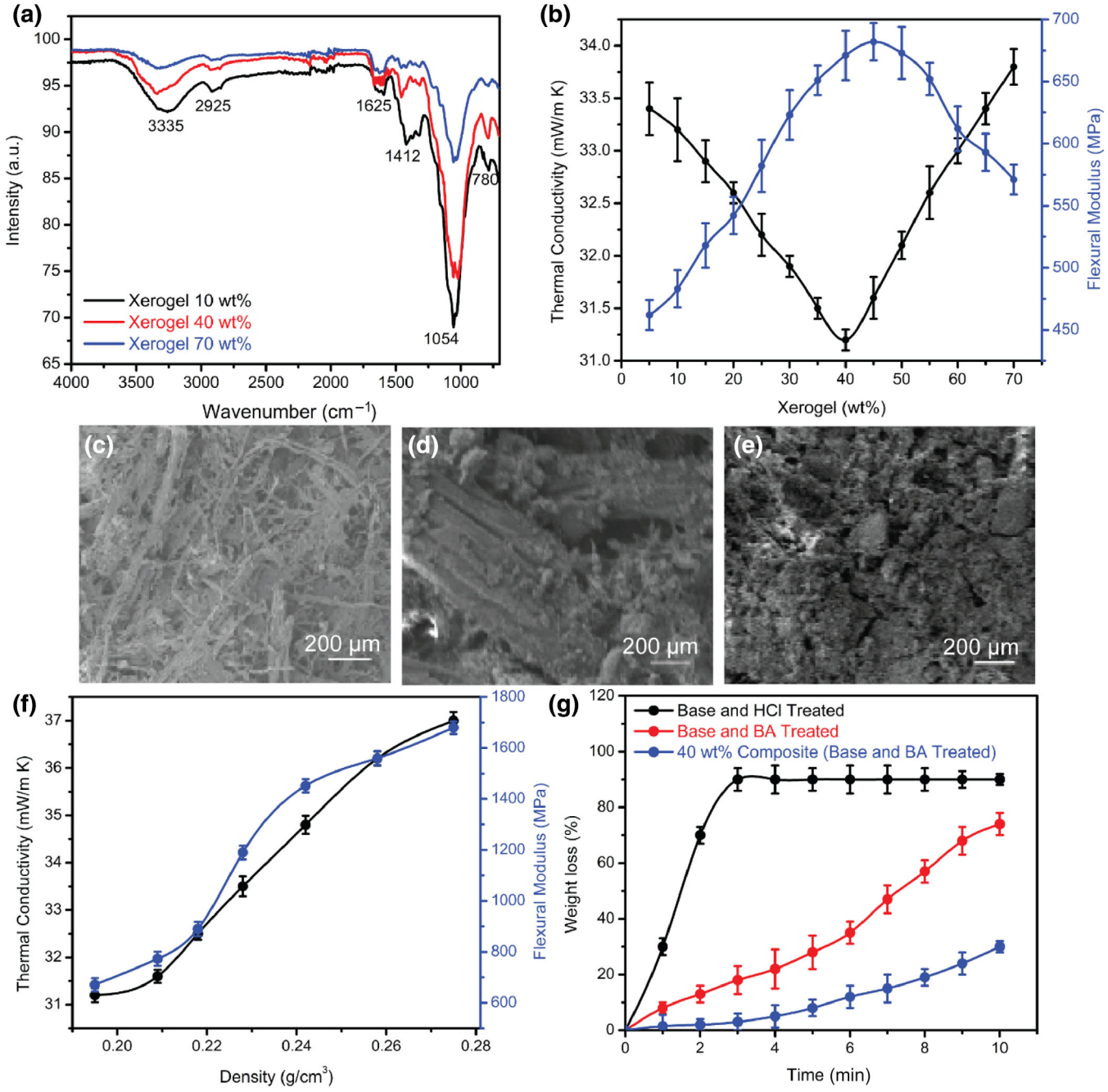

FIGURE 3 (a) Fourier-transform infrared spectroscopy spectra of different xerogel wt% of xerogel–cellulose composites, (b) thermal conductivity versus flexural modulus plot of different xerogel wt% of xerogel–cellulose composites, (c) scanning electron microscopy (SEM) image of 10 wt% xerogel–cellulose composite, (d) SEM image of 40 wt% xerogel–cellulose composite, (e) SEM image of 70 wt% xerogel–cellulose composite, (f) density-dependent study for 40 wt% xerogel–cellulose composite, (g) fire testing comparison between different composites. [Color figure can be viewed at wileyonlinelibrary.com]

flexural modulus of the composites increases from 468 to 682 MPa with increasing xerogel concentration from 5 to 45 wt% and then decreases to 570 MPa because of the increased density above 40 wt%. Figure 3f represents the density-dependent study of 40 wt% xerogel-cellulose nanocomposites. From Figure 3f, it is evident that the thermal conductivity and density of the composite are influenced by the different degrees of compression of the composites. The thermal conductivity of the composite increases from 31.2 to 36.6 mW/m K by increasing the compression which results in an increased density. The increased density leads the composite to get overly packed, promoting heat transfer through solid contacts and increasing thermal conductivity.

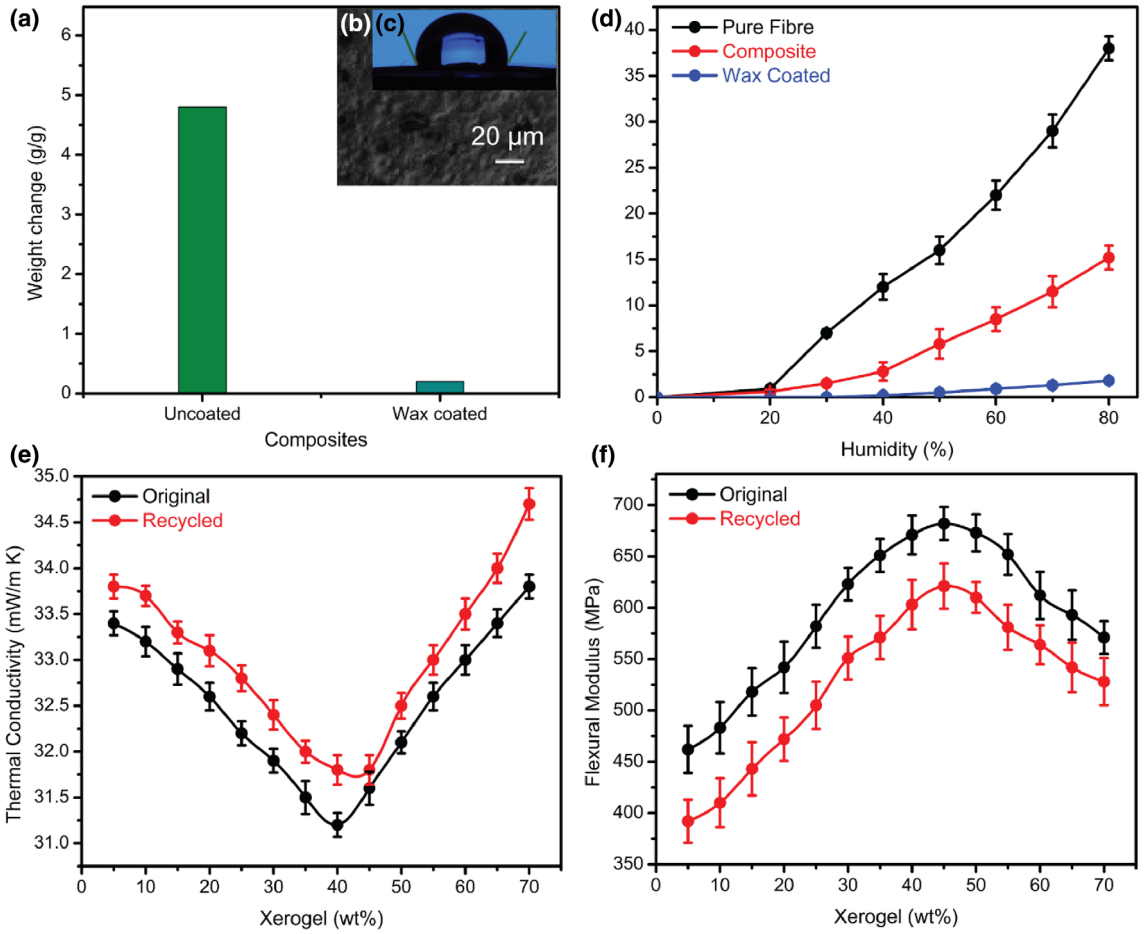

FIGURE 4 (a) Change in water absorption capacity for wax coated and uncoated xerogel–cellulose composite, inset (b) water contact angle for the wax coated composite, inset (c) scanning electron microscopy image of wax coated composite. (d) Thermal conductivity versus humidity (%) plot of pure cellulose fiber, wax coated and uncoated composites (e), (f) reusability test of xerogel–cellulose composites. [Color figure can be viewed at wileyonlinelibrary.com]

Fire retardancy is a very important criterion for biogenic materials and boric acid treatment plays a key role to improve the fire retardancy of cellulose–xerogel nanocomposites. Figure 3g shows the fire retardancy of 40 wt % xerogel–cellulose composites. From Figure 3g, the boric-acid-treated xerogel–cellulose composite show a small weight loss of around 30%, as compared with the base-boric acid treated (74%) and base-HCl treated (90%) samples over a period of burning time of 10 min which indicates that the boric acid, as well as silica xerogel, significantly improves the fire resistance of the composite due to the char formation (Figure S10). Water absorption capacity and wettability are other important factors considering the longevity of the biogenic composites. Figure 4a illustrates the water absorption capacity and wettability of wax-coated and uncoated xerogel-cellulose composite. Figure 4a shows that the wax-coated composite has a significantly lower water absorption capacity than that of the uncoated composite, indicating that the wax-coated composite has a developed degree of resistivity toward absorption through hydrophobic wax coating. Additionally, Figure 4a inset displays a water contact angle of 115^0 for the wax-coated composite, further confirming its hydrophobic nature. Figure 4b displays the surface morphology of the wax-coated composite, which reveals the presence of wax layer on the surface of the composite. The humidity-dependent thermal insulation study of the as-prepared composites is shown in Figure 4c. The humidity-dependent study is carried out by exposing the composites to different humidity levels using a programmable humidity controller and testing the thermal conductivity of each sample. Figure 4c compares the increment of thermal conductivity of with and without wax-coated xerogel-cellulose composite. The highest increase in thermal conductivity (approximately 37%) is observed in the case of pure cellulose fiber. On the other hand, the uncoated and wax-coated composite exhibit changes of 12% and 2%, respectively, indicating the role of the hydrophobic coating in reducing water absorption capacity and preventing an

increase in thermal conductivity. Furthermore, Figure 4d,e represents the reusability and recyclability of the as-prepared composite which shows the recovery percentage of thermal conductivity and flexural modulus are approximately 92% and 83%, respectively, indicating the high reusability and long-term availability of the as-prepared xerogel-cellulose composites.

3 | CONCLUSION

In this work, we present the synthesis of fire-retardant xerogel-cellulose nanocomposites from recycled hemp fibers and silica xerogel. Boric acid treatment has been used to improve the fire retardancy of the composites. Moreover, the structural properties of the as-prepared composites depend on the weight percentage (wt%) of silica xerogel and increasing the xerogel content up to 40 wt % has shown superior thermal insulation and mechanical properties. The as-prepared composites exhibit low thermal conductivity (31.2 mW/m K), high porosity (90%), superhydrophobicity, and reusability (with a recovery percentage of 92% for thermal insulation and 85% for flexural modulus). The combination of flame retardancy, high porosity, low thermal conductivity, good mechanical strength, and superhydrophobicity of as-prepared composites shows a promising way for effectively utilizing agricultural waste by-products in the form of carbon-sequestering building thermal insulation materials.

4 | EXPERIMENTAL

4.1 | Materials

Sodium dodecyl sulfate (SDS), urea, and reagent grade sodium silicate solution and water glass were purchased from Sigma-Aldrich. Hemp fibers were obtained from "Buffalo botanicals". Sodium hydroxide (NaOH) pellets, boric acid, and hydrochloric acid (HCl) were purchased from Fischer Scientific. Wax was purchased from Anchor seal 2. All the chemicals are analytical-grade and were used without further purification.

4.2 | Alkaline and acid treatment of hemp fiber

Initially, 40 g of hemp fiber was taken and blended using a regular blender with 1 L of deionized (DI) water. In the next step, the blended fibers were poured into a beaker, and NaOH pellets were added in desired concentrations (0.25, 0.5, 0.75, 1, 1.25, 1.5, 1.75, 2, 2.25, 2.5, 2.75, and 3 M). After NaOH addition, the alkaline solution was kept for stirring at 60°C for different time periods (30 min, 1 h, 1 h 30 min, 3 h, 4 h 30 min, 6 h, 7 h 30 min, and 9 h). After the treatment, the fibers were filtered and washed using DI water in a nylon net. The washing was done until the pH of the fibers became neutral.

For the acid treatment, 2 M–3 h NaOH-treated fibers were taken into a beaker and 200 mL DI water was added to it. After that, 0.5 M HCl was added to the solution until the pH becomes 5.0. Next, the acidic solution was kept stirred at 60°C for a desired period of time (15 min, 30 min, 1 h, 1 h 30 min, 2 h, 2 h 30 min, and 3 h). Similar to the alkaline treatment, HCl-treated fibers were also washed using nylon net and DI water.

In the case of boric acid treatment, the alkaline treated fibers (20 g) were taken into a beaker, and 200 mL of DI water was added to it. After that, 2 g of boric acid was added into the solution to make the pH of the solution 5 and stirred the mixture for a desired period of time (15 min, 30 min, 1 h, 1 h 30 min, 2 h, 2 h 30 min, and 3 h). Next, the fiber was filtered out using a nylon net. In all the cases of the fiber treatment procedure, the filtered fibers were dried in a preheated oven at 60°C at ambient pressure.

4.3 | Synthesis of silica xerogel precursor

At first, 1 g of SDS and 9.0 g (0.15 M) of urea were dissolved in 100 mL of DI water and agitated for 3 h at room temperature. Once the mixture achieved a uniform consistency, 11 mL of sodium silicate solution was added, and the solution was stirred for an additional 15 min. Subsequently, 2 M HCl solution was slowly added into the mixture until the pH of the solution becomes 9.0. The resulting solution was then placed in a preheated oven at 60°C at ambient pressure overnight for gelation.

4.4 | Purification procedure

To purify the xerogel precursor, 2 L of DI was added with the silica xerogel, and the mixture was thoroughly mixed using a mechanical agitator and left at a temperature of 60°C at ambient pressure for 24 h. Once a visible phase separation occurred, the upper transparent water portion was carefully removed while ensuring that the gel portion remained intact. This process was repeated four times until the water portion of the phase separation became clear, indicating successful purification.

4.5 | Synthesis of the xerogel-hemp fiber composite

At first, 20 g of blended alkaline-boric acid-treated hemp fibers were mixed with 200 mL of silica xerogel. The proportions of the fibers and silica xerogel were adjusted to create different weight percentages of cellulose–xerogel composites. Next, 3 L of DI water was poured into the mixture and stirred using a mechanical agitator for 30 min in order to achieve homogeneity. After that, the mixture was transferred to a paper-making setup. The paper-making setup uses a vacuum filtration methodology for making composites. Once the composite was formed, it was kept between two metallic perforated sheets, which were secured with screws to maintain the composite's thickness and prevent buckling. Finally, the composite was placed in a preheated oven at 60°C at ambient pressure for drying.

4.6 | Wax coating

Wax was added to DI water in 50:50 (wt/wt) ratio and stirred for 30 min to make a mixture. The mixture was then spray-coated on the composites. The spray-coated composites were dried at 60°C oven for 2 h at ambient pressure.

4.7 | Recycling

Cellulose–xerogel composites were broken into pieces and 1.5 L of DI water was added to it. The mixture was blended, and the slurry was transferred to the paper-making machine for re-making the composites. Similar to the original composites, the recycled composites were sandwiched between perforated sheets to maintain thickness and prevent buckling, dried in a preheated oven at 60°C.

4.8 | Physical measurements

Flexural modulus was used as a property to study the mechanical strength of the samples and uniaxial flexural modulus tests of specimens, prepared with bulk dimensions of 120 mm × 120 mm × 8 mm, using a universal test system (Model SSTM-20KN from United Testing Systems) for testing samples up to 500 N. The steady-state methodology is used to measure the thermal conductivity of the composite samples. This measurement is conducted using the heat flow meter—100 series (HFM-100) thermal conductivity measurement system from Thermtest. The system adheres to the ASTM C518 standard. The system determines the thermal conductivity of the tested material once the heat flux between the clamping plates and through the specimen stabilizes at a constant value over time. Samples with dimensions of 120 mm × 120 mm × 8 mm were tested for thermal conductivity values. The calculation of the bulk density or the amount of hemp fiber and xerogel composites within a given volume was performed using Equation (1).

$$\rho = m/V. \tag{1}$$

The porosity of the hemp-xerogel samples was determined using Equation (2), where ρ_m represents the bulk density obtained from the ratio of weight to volume, and ρ_s indicates the skeletal density determined using the pycnometer system (Micromeritics Accu-Pyc II 1340). The equation for porosity calculation is shown as follows:

$$\text{Porosity}\,(\%) = (1 - \rho_m/\rho_s) \times 100. \tag{2}$$

FTIR (Agilent carry 560) was employed to analyze the chemical bonding state of finely ground xerogel samples, as well as the interfacial bonding of hemp fiber treated under different process conditions. The microstructure of the cellulose sample and the xerogel/cellulose composites were examined using a focused ion beam scanning electron microscope (FIB-SEM, Carl Zeiss AURIGA Crossbeam). In addition, TGA was conducted using the TA Instrument DSC SDT Q600 to assess thermal stability. The TGA analysis was conducted in N_2 atmosphere with a heating rate of 10°C/min. Fire testing of samples was carried out by clamping the composites and providing flame through a candle. The weight was recorded after each 1 min interval for 10 min.

AUTHOR CONTRIBUTIONS

Porus Sunil Jadhav: Data curation (lead); investigation (lead); methodology (lead); writing – review and editing (supporting). **Arpita Sarkar:** Data curation (supporting); investigation (supporting); writing – original draft (lead). **Long Zhu:** Data curation (supporting). **Shenqiang Ren:** Conceptualization (lead); funding acquisition (lead); supervision (lead).

ACKNOWLEDGMENTS

Shenqiang Ren acknowledges the funding support on this work by the United States Department of Energy (DOE) Advanced Research Projects Agency-Energy (ARPA-E) award DE-AR0001771.

DATA AVAILABILITY STATEMENT

The data that supports the findings of this study are available in the supplementary material of this article.

ORCID

Arpita Sarkar https://orcid.org/0000-0001-7375-8793
Shenqiang Ren https://orcid.org/0000-0002-9987-3316

REFERENCES

[1] M. Viel, F. Collet, C. Lanos, *Ind. Crops Prod.* **2018**, *120*, 214.
[2] N. Husing, U. Schubert, *Angew. Chem., Int. Ed.* **1998**, *37*, 23.
[3] A. C. Pierre, G. M. Pajonk, *Chem. Rev.* **2002**, *102*, 4243.
[4] H. Maleki, N. Hüsing, *Appl. Catal., B* **2018**, *221*, 530.
[5] S. Amaducci, D. Scordia, F. H. Liu, Q. Zhang, H. Guo, G. Testa, S. L. Cosentino, *Ind. Crops Prod.* **2015**, *68*, 2.
[6] C. Schluttenhofer, L. Yuan, *Trends Plant Sci.* **2017**, *22*, 917.
[7] T. Karche, R. M. Singh, *Turk. J. Bot.* **2019**, *43*, 710.
[8] S. Duquesne, F. Samyn, P. Ouagne, S. Bourbigot, *J. Ind. Text.* **2015**, *44*, 665.
[9] A. Rachini, G. Mougin, S. Delalande, J. Y. Charmeau, C. Barres, E. Fleury, *Polym. Degrad. Stab.* **2013**, *97*, 1988.
[10] R. Kozlowski, M. Wladyka-Przybylak, *Polym. Adv. Technol.* **2008**, *19*, 446.
[11] A. Samir, F. H. Ashour, A. A. A. Hakim, M. Bassyoun, *npj Mater. Degrad.* **2022**, *6*, 68.
[12] L. Yu, J. Cai, H. Li, F. Lu, D. Qin, B. Fei, *BioResources* **2017**, *12*, 5296.
[13] P. Moreno, N. Villamizar, J. Perez, A. Bayona, J. Roman, N. Moreno, N. S. M. Cardozo, *Clean Technol. Enviro. Policy* **2021**, *23*, 1537.
[14] M. Liu, D. Fernando, G. Daniel, B. Madsen, A. S. Meyer, M. T. Ale, A. Thygesen, *Ind. Crops Prod.* **2015**, *69*, 29.
[15] M. J. Peña, C. E. Vergara, N. C. Carpita, *Advanced Dietary Fibre Technology*, Blackwell Science, Cambridge, UK **2008**, p. 42.
[16] N. C. Carpita, D. M. Gibeaut, *Plant J.* **1993**, *3*, 1.

SUPPORTING INFORMATION

Additional supporting information can be found online in the Supporting Information section at the end of this article.

How to cite this article: P. S. Jadhav, A. Sarkar, L. Zhu, S. Ren, *J. Appl. Polym. Sci.* **2024**, *141*(12), e55137. https://doi.org/10.1002/app.55137